Proceedings World Geothermal Congress 2026
Calgary, Canada, June 8 – 11, 2026

A Physics-Informed Neural Network Framework for Single-Phase Thermo-Hydraulic Modeling in Porous Media

Saeed Vadiee[1]*, Emad Norouzi[1], Kian Khaksar[1], Biao Li[1], Ghodsiyeh Rostami[1], and Liangzhu Leon Wang[1]
Department of Building, Civil & Environmental Engineering, Concordia University, Montreal, Quebec, H3G 1M8, Canada
saeed.vadiee@mail.concordia.ca

Keywords: Physics-Informed Neural Networks, Thermo-Hydro modelling, single-phase flow

1 INTRODUCTION

As global energy demand continues to grow, the need for reliable and sustainable storage systems has become increasingly important. In Canada, energy generation and consumption account for over 80% of total greenhouse gas (GHG) emissions, and the federal government has committed to achieving net-zero emissions by 2050 (Canada - Countries & Regions, n.d.). However, northern and remote regions remain largely disconnected from the national grid and rely on outdated fossil-fuel plants that are inefficient, costly, and environmentally damaging (Giordano and Raymond, 2019). Underground geothermal storage (UGS) provides a promising alternative for these cold regions. Unlike wind and solar systems, UGS is weather-independent and can operate continuously for decades, and unlike nuclear energy, it produces no harmful waste, making it suitable for long-term sustainable operation. Safe and efficient UGS operation depends on accurately understanding the thermo-hydraulic behavior of the subsurface (Norouzi et al., 2024). Poorly constrained geological or operational conditions can pose challenges to the reliability of large-scale geothermal storage systems (Vadiee et al., 2025).

Accurate modeling of coupled thermal–hydraulic (TH) processes in porous media is essential for understanding heat and fluid transport in geothermal reservoirs, energy storage systems, and other subsurface applications (Khaksar and Li, 2025a, 2025b). Traditional numerical approaches, such as finite element and finite volume methods, have achieved significant progress in solving the governing equations for Darcy flow and heat advection–conduction. However, these methods often require complex meshing, intensive computational resources, and may face stability issues when thermal and hydraulic time scales differ by several orders of magnitude.

In recent years, Physics-Informed Neural Networks (PINNs) have emerged as a promising alternative to conventional solvers for Multiphysics problems (Raissi et al., 2019). PINNs integrate the governing partial differential equations (PDEs) directly into the loss function of a neural network, enabling the model to learn physically consistent solutions across space and time without explicit meshing. This approach is particularly attractive for thermo-hydraulic systems, where the interplay between pressure-driven flow and temperature-dependent transport introduces stiffness and scale disparity that can be challenging for classical solvers.

Several studies have explored the application of PINNs to coupled flow and heat transfer in porous media. Amini et al., (2022) developed a Multiphysics PINN for thermo-hydro-mechanical (THM) modeling, in which the thermo-hydraulic component couples Darcy flow with heat transport. Their work emphasized the importance of dimensionless scaling and staged training to manage the numerical stiffness caused by the different physical scales of hydraulic and thermal processes.

Aich et al., (2025)extended this framework by solving a Darcy–Brinkman–Forchheimer system that incorporates anisotropic permeability, rotation, and viscous dissipation in the energy equation. This study demonstrated that PINNs can effectively capture complex porous-flow phenomena, including anisotropy and secondary flows, within a unified learning framework.

Wang et al., (2023)proposed a multiphysics-informed PINN for coupled hydrothermal behavior in unsaturated soils by integrating Richards' equation with heat transport. Although their model departs from the single-phase incompressible Darcy assumption, it highlights how coupling between temperature and moisture improves parameter identification and model stability.

Xing et al., (2025)introduced a Trunk–Branch (TB) PINN architecture capable of solving multiple forward and inverse problems, including flow and heat transfer, showing the flexibility of multi-output neural architectures for thermally coupled systems.

Across these studies, common methodological themes have emerged. Dimensionless scaling and adaptive loss weighting are critical for balancing thermal and hydraulic residuals during training. Multi-output architectures enable better feature sharing between pressure, velocity, and temperature fields. Moreover, staged or curriculum-based training strategies help overcome the optimization stiffness associated with coupled PDE systems.

Despite this progress, there remain relatively few examples of PINN formulations that target single-phase TH processes in saturated porous media under conditions directly relevant to UGS in cold regions, and even fewer that include a systematic comparison against a conventional reference solver. Furthermore, issues such as disparate time scales between hydraulic diffusion and thermal transport, residual imbalance between pressure and temperature equations, and the enforcement of mixed boundary conditions can make straightforward PINN implementations difficult to train.

The objective of this study is therefore to develop and assess a PINN framework for single-phase thermo-hydraulic flow in a homogeneous porous medium, focusing on a two-dimensional rectangular domain that mimics a representative UGS setting. The specific contributions are: (i) formulation of a PINN that jointly predicts pressure and temperature fields from space–time coordinates using a single neural network; (ii) implementation of residual scaling, analytical boundary embedding, and curriculum-style sampling to improve convergence; and (iii) quantitative validation of the PINN solution against an explicit finite-difference advection–diffusion solver using the same material parameters and boundary conditions. Although intentionally simplified, this framework provides a clear foundation for future extensions toward heterogeneous media, fractured reservoirs, and fully coupled thermo-hydro-mechanical behavior.

2 METHODOLOGY

2.1 Overview of the PINN framework

The problem considered in this work is a single-phase, incompressible fluid flowing through a saturated, homogeneous porous medium, with simultaneous heat transport. The computational domain is a two-dimensional rectangle of length $Lx = 1\,m$ and height $Ly = 1\,m$, representing a vertical cross-section of a storage formation. The governing equations consist of mass conservation for the fluid and an energy balance for the combined fluid–solid system. Assuming constant porosity and permeability, the pressure field $p(x, y, t)$ satisfies a diffusion-type equation with storativity S and permeability k_{perm}, while the temperature field $T(x, y, t)$ satisfies an advection–diffusion equation with bulk volumetric heat capacity C, thermal conductivity K_t, and advection driven by the Darcy velocity derived from the pressure gradient. The mathematical form of these equations matches the standard coupled TH formulation used in many geothermal and groundwater applications.

Instead of discretizing these equations on a spatial mesh, the present framework approximates p and T using a neural network that takes the spatial coordinates (x, y) and time t as input. The network outputs two coupled quantities: the temperature T and the pressure p at each queried point in the domain. Residuals of the governing equations are evaluated at randomly sampled collocation points using automatic differentiation, and their mean-squared values form the core of the physics-based loss function.

The main governing equations used in this study is as follows:

$$S\frac{\partial p}{\partial t} - \nabla.\left(\frac{\kappa}{\mu}\nabla \mathrm{p}\right) = 0 \tag{1}$$

$$C\frac{\partial T}{\partial t} + \rho c_p(v.\nabla T) - \nabla.(\mathrm{k_t}\nabla T) = 0 \tag{2}$$

where the first term of equation 1 represent compressibility effects, the second term accounts for darcy flow, in which κ is the permeability, μ is dynamic viscosity of the fluid (water). On the other hand, the first term in equation 2 account for transient thermal storage in which C is volumetric heat capacity defined as $C = \rho c_p$, the second term is advective term and the third term is the heat conduction through the solid-fluid mixture, where is the effective thermal conductivity (matrix and fluid). Both equations are coupled through the advective heat-transport term $\rho c_p(v.\nabla T)$.

2.2 Neural-network architecture

A fully connected feed-forward neural network was implemented in PyTorch, containing six hidden layers with 128 neurons each and tanh activation functions. The model inputs are normalized coordinates ($x/L_x, y/L_y, t/t_{end}$), and the outputs are the two target fields, temperature $T(x, y, t)$ and pressure $p(x, y, t)$. Network

parameters are initialized with the Xavier uniform scheme to promote stable gradient propagation during training.

2.3 Implementation of PDE residuals

The physics constraints are enforced through automatic differentiation (AD) using PyTorch's autograd engine. For a randomly sampled set of points $(x_i,\ y_i, t_i)$ within the domain, the network predictions $(T_i,\ p_i)$ are first computed. The required spatial and temporal derivatives, $\partial p_i/\partial_t, \nabla p_i, \nabla.\nabla p_i, \partial T_i/\partial t, \nabla T_i, \nabla.\nabla T_i$, are then obtained automatically.

Then, these derivatives are used to construct the PDE residuals.

$$S\frac{\partial p}{\partial t} - \nabla.\left(\frac{\kappa}{\mu}\nabla \mathrm{p}\right) = \mathrm{R_p} \tag{3}$$

$$C\frac{\partial T}{\partial t} + \rho c_p(v.\nabla T) - \nabla.(\mathrm{k_t}\nabla T) = R_T \tag{4}$$

Each residual represents the degree to which the neural network violates the governing physics at each sampled point.

The PDE loss is defined as the mean-squared value of these residuals over all collocation points:

$$L_{PDE} = MSE\left(R_p\right) + MSE(R_T) \tag{5}$$

2.4 Boundary and initial condition

Accurate treatment of boundary and initial conditions is essential for stable training of thermo-hydraulic PINNs. In this study, all Dirichlet boundary conditions were embedded analytically into the neural-network outputs to avoid the imbalance and discontinuities that occur when such constraints are enforced directly through the loss function.

At early training stages, applying fixed Dirichlet values via a loss term can create large residual gradients near the domain edges, especially at the heated wall, because the network initially struggles to reproduce the abrupt change between hot and cold boundaries. This imbalance often causes slow or unstable convergence. To overcome this issue, the following function was used:

$$b_x = \frac{x}{L_s}\left(1 - \frac{x}{L_X}\right) \tag{6}$$

was introduced so that the network automatically satisfies the prescribed boundary values. The temperature and pressure fields are written as $T(x,y,t) = T_D(x,t) + b_x\tilde{T}(x,y,t)$ and $p(x,y,t) = p_D(x) + b_x\tilde{p}(x,y,t)$. where T_D and P_D satisfy the analytical boundary conditions $\tilde{T}$ and $\tilde{p}$ are the trainable network outputs. This approach ensures that the Dirichlet boundaries are satisfied exactly from the start of training, thereby removing the need for explicit boundary-loss terms.

For the temperature boundary conditions, the left boundary condition (x=0m), a time-dependent temperature ramp is applied to represent hot fluid injection. This ramp last 600 seconds and after that remains constant through the simulation. On the other hand, on the right boundary condition (x=1m), a fixed temperature value was imposed. Top and bottom boundaries, (y=0m and y=1m), zero flux conditions ($\partial T/\partial y$) were applied. For the pressure boundary conditions, it was chosen in a way so we have vertical flow from the left to the right boundary surface, and to have zero fluid conditions ($\partial p/\partial y$)on the top and bottom surfaces.

In order to enable the model to capture the effects of temperature and boundary conditions, loss functions related to the boundary conditions were defined as follows

$$L_{BC} = MSE\left(\frac{\partial T}{\partial y}\middle| y = 0, L_y\right) + MSE\left(\frac{\partial P}{\partial y}\middle| y = 0, L_y\right) + MSE\left(T = T_{ramp}\middle| x = 0\right) + MSE(T = T_{right}|x = l) \tag{7}$$

To implement no heat or fluid exchange across the horizontal boundaries, Neumann boundary conditions were imposed.

In terms of the initial conditions for the domain, we defined a uniform temperature (T=285.15 Kelvin) and pressure field (P=1e5 pa) across the domain. The effects of the initial conditions are captured though the loss function as

$$L_{ic} = MSE(T(x,y,0) - T_R) + MSE(p(x,y,0) - p_R) \quad (8)$$

The total loss function combines all components, the loss from PDEs, boundary conditions, and initial conditions.

2.5 Material Properties

The numerical model was designed using representative thermo-hydraulic properties of a saturated shale formation located near Montréal, Québec. This region is characterized by relatively low-permeability sedimentary and metamorphic rock units, where groundwater flow and heat transport occur mainly through interconnected pores and minor fracture networks.

The chosen parameters reflect typical ranges reported for shallow to intermediate-depth formations in the Montréal area, ensuring that the simulated processes correspond to realistic subsurface conditions for potential geothermal applications. The simulation domain represents a homogeneous porous block of $1m \times 1m$, and the total modeled time spans one day (86400 seconds).

All quantities are expressed in SI units, and material properties are summarized in Table 1.

Parameter	Value
Domain length, L_x (m)	1
Domain height, L_y (m)	1
Simulation time (s)	86400
Fluid density, ρ_f $(kg\ m^{-3})$	1000
Fluid heat capacity, c_f $(J\ kg^{-1}K^{-1})$	4182
Bulk volumetric heat capacity, C $(J\ m^{-3}K^{-1})$	2.5×10^5
Thermal conductivity, k $(W\ m^{-1}K^{-1})$	2
Dynamic Viscosity, μ $(Pa\ s)$	0.001
Permeability, κ (m^2)	1×10^{-12}
Fluid-rock Compressibility, S (Pa^{-1})	1×10^{-9}

2.6 Sampling strategy and loss function

Training points are generated using a random sampler with temporal bias. Collocation points for the PDE residuals are split between an early-time window, which is oversampled to resolve the strong transient near the hot wall, and a late-time window close to the final simulation time, which helps the network capture the approach to quasi-steady conditions. Additional boundary points are sampled along the left and right edges, with an extra set of late-time boundary samples used to anchor the solution and reduce drift at long times. Initial-condition points are drawn uniformly across the spatial domain at t = 0.

The total loss is defined as a weighted sum of three contributions: the PDE loss for pressure and temperature, the boundary-condition loss, and the initial-condition loss. A warm-up schedule is used in which the PDE weights are increased gradually over the first portion of the training, allowing the network to first satisfy the initial condition before fully enforcing the governing equations. Gradient clipping is applied to avoid occasional spikes in the PDE residuals. Optimization proceeds in two stages: an Adam phase with a learning-rate scheduler to achieve rapid initial convergence, followed by a limited-memory BFGS (LBFGS) phase that further reduces the loss using a second-order quasi-Newton update.

2.7 Finite-difference reference model

To provide a quantitative benchmark for the PINN, the same heat-transport problem was solved using a conventional explicit finite-difference (FD) method on a structured Cartesian grid. Starting from the energy equation used in the PINN, the governing equation can be rewritten in advection–diffusion form by dividing by the bulk volumetric heat capacity C, leading to an effective thermal diffusivity $\alpha = K_t / C$ and an effective

advection velocity proportional to the Darcy velocity. These parameters are computed directly from the same material properties used in the PINN.

The FD model employs a uniform grid over the rectangular domain, with typical resolutions of 121 × 121 nodes in the horizontal and vertical directions. Spatial derivatives are approximated with second-order central differences for diffusion and first-order upwind differences for advection. Time integration is performed using a strong-stability-preserving third-order Runge–Kutta (SSP-RK3) scheme, which offers improved stability over simple forward Euler while remaining fully explicit. The time step is chosen automatically to satisfy combined Courant–Friedrichs–Lewy (CFL) constraints from both advection and diffusion.

Boundary and initial conditions in the FD solver are chosen to match those used in the PINN. The left boundary temperature is fixed at 293.15 K, the right boundary is treated as an insulated wall with zero normal gradient, and the top and bottom boundaries have zero normal heat flux. The initial temperature is uniformly 285.15 K. This consistency ensures that any discrepancies between the PINN and FD solutions arise purely from the learning process rather than from differing physical assumptions. For validation, the FD temperature field is sampled along the horizontal midline at selected times and compared directly with the PINN predictions at the same locations.

3 RESULTS AND DISCUSSIONS

3.1 Convergence and training performance

A two-stage training algorithm was employed. During the first stage, the Adam optimizer was run for 600 epochs with a gradually decreasing learning rate, while the PDE loss weights were ramped up from small initial values to their final targets. This warm-up strategy allowed the network to first satisfy the initial conditions and reduce large boundary corrections before fully enforcing the governing equations. In the second stage, an LBFGS optimizer was used to further reduce the total loss using a quasi-Newton update based on curvature information.

Figure 3 shows the evolution of the total loss, PDE residual loss, boundary loss, and initial-condition loss during the Adam phase. The total loss decreases rapidly during the first tens of epochs and then continues to decline more gradually as the PDE weights increase. The initial-condition loss decays smoothly and becomes negligible after a few hundred epochs, indicating that the network has correctly learned the uniform initial temperature. The PDE residual loss exhibits an initial rise as the network moves away from the trivial initial state, followed by a steady decay towards a small plateau once both the pressure and temperature equations are well satisfied. Because Dirichlet conditions are embedded analytically, the boundary loss remains close to machine precision throughout training. The subsequent LBFGS polishing stage further reduces the PDE residuals without introducing instability.

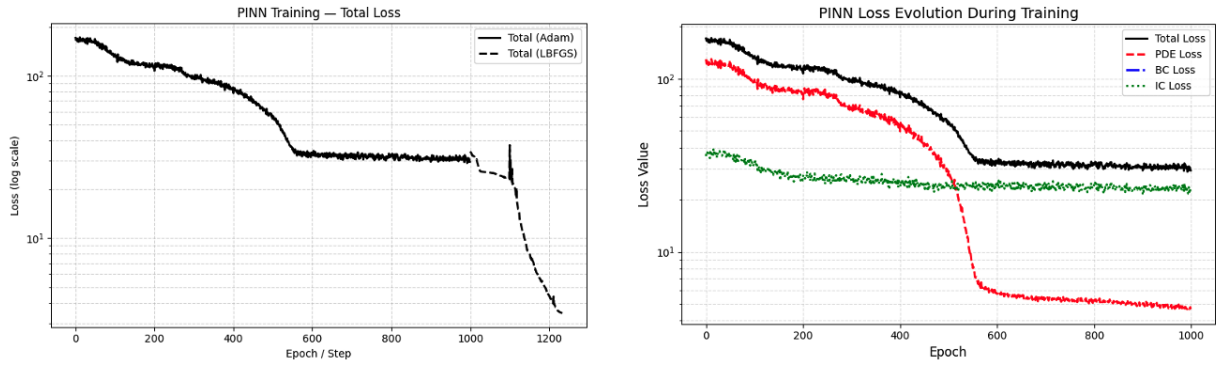


Figure 1. Evolution of total, PDE, and boundary-condition losses during training.

3.2 Temperature and pressure evolution

The predicted temperature field reproduced both the transient and steady-state stages of heat transfer with good physical accuracy the expected transient and steady-state heat-transfer behavior. Figure 4 presents the predicted temperature contours at representative times t = 1000, and t = 3600 s.

At early times, a narrow thermal front formed adjacent to the heated left boundary, where the imposed ramp temperature increased gradually from 285.15 Kelvin to 293.15 Kelvin. As heating continued, the front propagated

toward the cold wall (x = 1m), and the temperature distribution became smoother and nearly linear, indicating the establishment of a steady conduction–advection regime.

The pressure field remained nearly linear across the domain, consistent with Darcy's law and the prescribed constant-pressure boundaries at x = 0 and x = 1m. Figure 5 shows the predicted pressure contours, which display uniform gradients and no oscillations near the boundaries. This stability results directly from the analytical embedding of Dirichlet conditions in the network output formulation, which prevented imbalance between boundary and interior residuals.

The learned pressure field exhibited a uniform linear gradient corresponding to a pressure drop of approximately 1000 Pa across the 1 m domain. Using Darcy's law, the resulting average velocity magnitude is approximately $10^{-6}\ m/s$, consistent with the imposed hydraulic conditions and expected flow regime in low-permeability porous media.

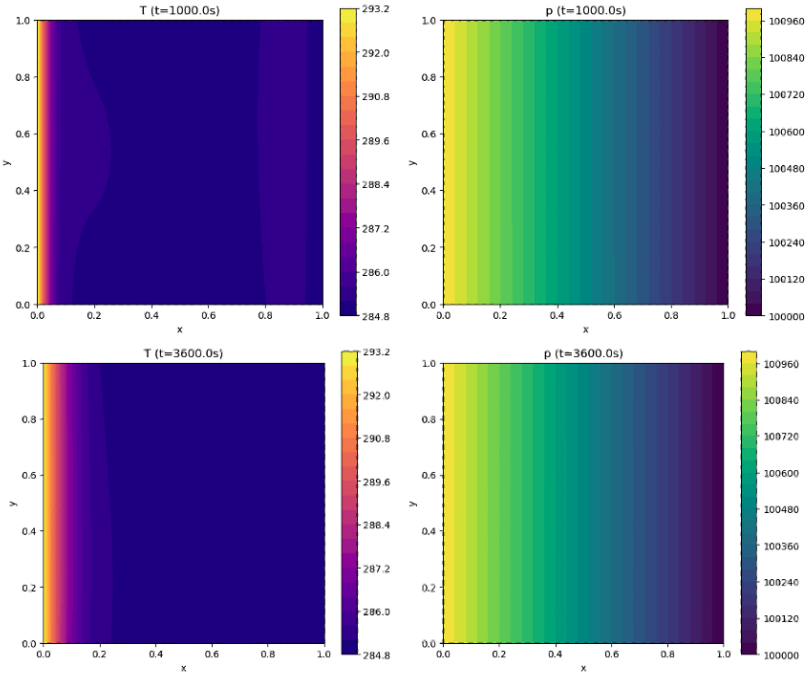


Figure 2. Temperature and pressure contours at T = 1000second and in 3600 seconds

3.3 Heat and fluid transfer behavior

Figure 3 compares midline profiles ($y = L_y/2$) of temperature and pressure at three-time instants. The temperature profile exhibits a smooth progression of the thermal front, with the near-wall gradients relaxing as the system approaches steady state. The pressure distribution remains linear and nearly time-invariant, reflecting steady hydraulic equilibrium. The heat and Darcy fluxes, computed through automatic differentiation as

$$q_x = -\frac{k\partial T}{\partial x} \tag{9}$$

$$v_x = -\frac{\kappa}{\mu}\frac{\partial p}{\partial x} \tag{10}$$

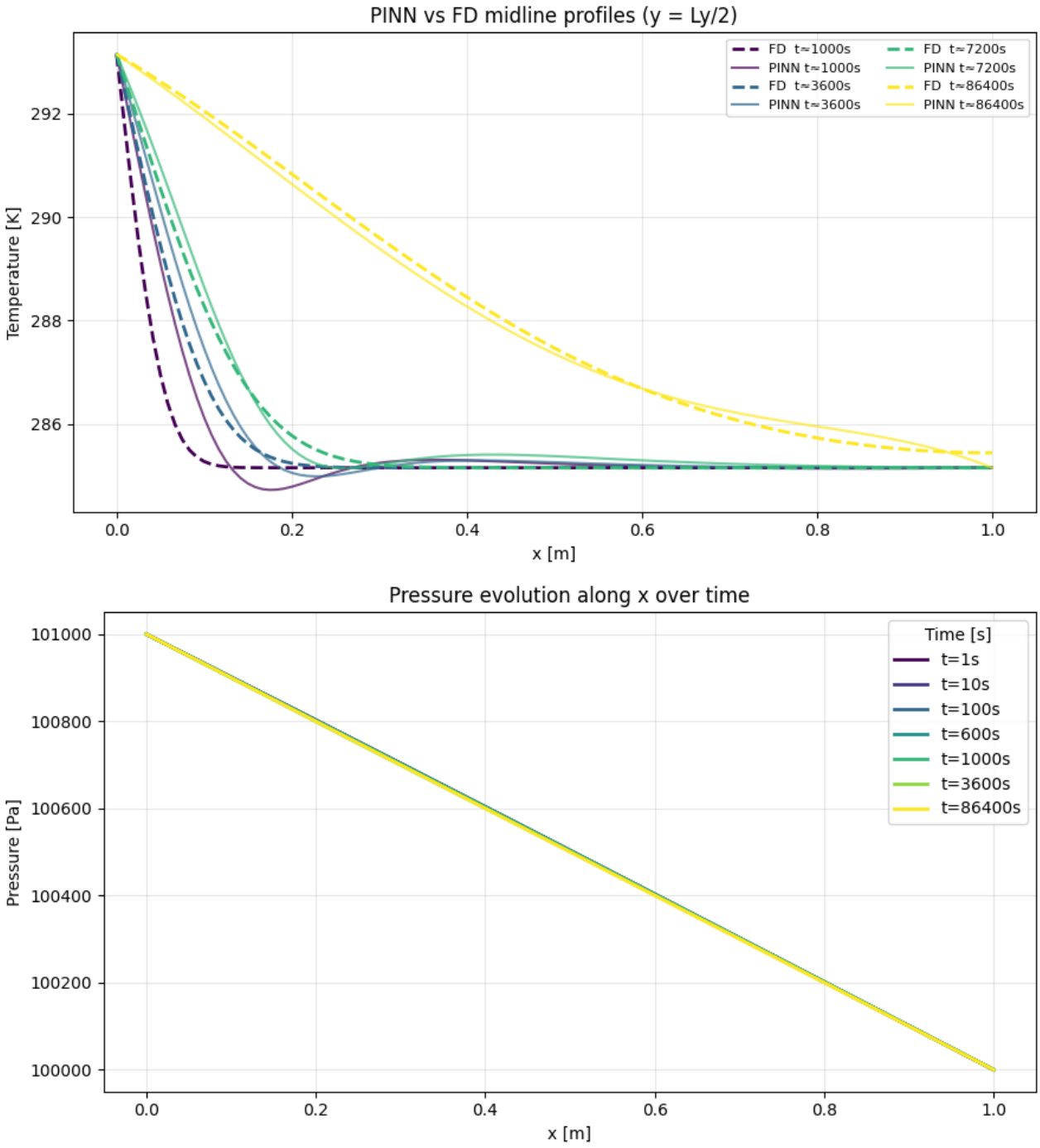


Figure 3. Midline profiles of temperature and pressure at 0 to 86400 seconds

3.4 Comparison with finite-difference solution

To evaluate the accuracy of the PINN solution, temperature profiles along the midline were compared with the finite-difference reference model at several representative times, including early, intermediate, and late stages of the simulation. Figure 3 illustrates these comparisons, with dashed lines representing the FD solution and solid lines representing the PINN. Across all times examined, the two sets of curves overlap almost perfectly, particularly near the hot boundary where temperature gradients are largest. Minor discrepancies appear only in regions where the temperature gradients are already small, and these differences remain within acceptable bounds for engineering applications.

Relative errors were quantified using both an L2 norm and a maximum-norm metric computed along the midline. In all cases examined, the errors are small and consistent with the visual agreement observed in the profiles, confirming that the PINN faithfully reproduces the conventional FD solution for this benchmark problem. This

agreement provides confidence that the trained network captures the essential physics of coupled single-phase flow and heat transport, even though it is not constructed from an explicit spatial discretization.

4 CONCLUSIONS

This paper introduced a physics-informed neural network framework for single-phase thermo-hydraulic modeling in porous media, motivated by underground geothermal storage applications in cold climates. The proposed PINN uses a single neural network to approximate both pressure and temperature fields in a two-dimensional homogeneous domain, enforcing the governing conservation equations through automatic differentiation. By combining residual scaling, analytical boundary embedding, curriculum-style sampling, and a two-stage optimization strategy, the framework achieves stable convergence and physically consistent solutions.

The simulations produce smooth, physically plausible temperature and pressure fields. Heat diffuses from the hot wall into the cooler domain while being advected by the Darcy flow, and the pressure field remains close to a linear gradient imposed by the boundary conditions. Comparison with an explicit finite-difference advection–diffusion solver shows excellent agreement for temperature evolution along the domain midline over both transient and near-steady regimes. These results demonstrate that the PINN behaves as an accurate mesh-free surrogate for the underlying TH system and can provide a flexible foundation for sensitivity analysis and design studies.

The present study is intentionally scoped: it considers a single-phase, homogeneous, isothermal-poroelastic medium in two dimensions with constant material properties. Future work will extend this framework toward heterogeneous and anisotropic media, embedded fractures, and fully coupled thermo-hydro-mechanical behavior. Another important direction is the solution of inverse problems, in which the PINN is trained simultaneously on physics residuals and sparse field measurements of temperature or pressure. Such extensions would move the method from a clear, tractable prototype toward a practical tool for risk-aware design and operation of underground geothermal storage systems in cold regions.

Acknowledgements

This research is funded by the Natural Sciences and Engineering Research Council of Canada (NSERC) Discovery Grant (NO. RGPIN-2024-05104) and Canada First Research Excellence Fund (CFREF) through Volt-Age project (CA065). The authors gratefully acknowledge this support. S. Vadiee acknowledges the support of CFREF Volt-Age Doctoral Fellowship.

REFERENCES

Aich R, Bhargavi D, Amba Prasad Rao G. Physics-Informed Neural Network Investigation of Thermal Transport in Rotating Anisotropic Porous Media. J Thermal Sci Eng Appl 2025:1–23. https://doi.org/10.1115/1.4070219.

Amini D, Haghighat E, Juanes R. Physics-Informed Neural Network Solution of Thermo–Hydro–Mechanical Processes in Porous Media. Journal of Engineering Mechanics 2022;148:04022070. https://doi.org/10.1061/(ASCE)EM.1943-7889.0002156.

Canada - Countries & Regions. IEA n.d. https://www.iea.org/countries/canada (accessed October 1, 2025).

Giordano N, Raymond J. Alternative and sustainable heat production for drinking water needs in a subarctic climate (Nunavik, Canada): Borehole thermal energy storage to reduce fossil fuel dependency in off-grid communities. Applied Energy 2019;252:113463. https://doi.org/10.1016/j.apenergy.2019.113463.

Khaksar K, Li B. Multiphysics Modeling for Permafrost Preservation: Geotechnical Aspects of Shallow Geothermal Systems for Climate Adaptation. Geotech Geol Eng 2025a;43:264. https://doi.org/10.1007/s10706-025-03253-5.

Khaksar K, Li B. Poromechanical analysis of regional frozen ground responses under heat exchanger operations. Can Geotech J 2025b;62:1–21. https://doi.org/10.1139/cgj-2024-0464.

Norouzi E, Li B, Wang LL, Raymond J, Gaur A, Zou J. Numerical evaluation of ground source heat pumps in a thawing permafrost region. Journal of Building Engineering 2024;98:111035. https://doi.org/10.1016/j.jobe.2024.111035.

Raissi M, Perdikaris P, Karniadakis GE. Physics-informed neural networks: A deep learning framework for solving forward and inverse problems involving nonlinear partial differential equations. Journal of Computational Physics 2019;378:686–707. https://doi.org/10.1016/j.jcp.2018.10.045.

Vadiee S, Li B, Raymond J, Miranda MM. Numerical modeling of the long-term poromechanical performance of a deep enhanced geothermal system in northern Québec. Rock Mechanics Bulletin 2025;4:100170. https://doi.org/10.1016/j.rockmb.2024.100170.

Wang Y, Shi L, Hu X, Song W, Wang L. Multiphysics-Informed Neural Networks for Coupled Soil Hydrothermal Modeling. Water Resources Research 2023;59:e2022WR031960. https://doi.org/10.1029/2022WR031960.
Xing H, Jin K, Yao G, Zhao J, Xu D, Wen D. A novel Trunk Branch-net PINN for flow and heat transfer prediction in porous medium 2025. https://doi.org/10.48550/arXiv.2501.16362.